PHYSICAL REVIEW D VOLUME 44, NUMBER 5 1 SEPTEMBER 1991

Rare decays of the top quark in the standard and two-Higgs-doublet models

G. Eilam
Department of Physics, Technion, Israel Institute of Technology, Haifa, 32000, Israel

J. L. Hewett
Department of Physics, University of Wisconsin, Madison, Wisconsin 53706

A. Soni
Department of Physics, Brookhaven National Laboratory, Upton, New York 11973
(Received 9 January 1991)

The decays $t \to cV$, where $V=\gamma$, g, or Z, and $t \to cH$ are calculated, keeping all masses, in the standard model (SM) for all possible values of the top-quark mass that are consistent with present data. We find that the branching fractions for these processes are small, the largest being $B(t \to cH) \sim 10^{-7}$ and $B(t \to cg) \sim 10^{-10}$. Our calculations are then extended to include the possible contributions of charged Higgs bosons to the transitions $t \to cV$ in the context of general two-Higgs-doublet models. These new contributions can enhance the SM branching fractions by as much as 3–4 orders of magnitude, e.g., $B(t \to cg) \sim 10^{-7}$–10^{-6}, for various values of the parameters. General expressions for flavor-changing neutral-current decays of heavy quarks including all masses and momenta, in the SM and in the two-Higgs-doublet models, are also given.

I. INTRODUCTION

Rare decays of heavy quarks have long been a subject of intense theoretical and experimental study. The prime rationale for this is the fact that loop processes are a powerful test for the short-distance structure of the theory. Furthermore, many such decays are sensitive to parameters in the standard model (SM) and are excellent probes for the effects of new physics, such as supersymmetry, charged Higgs bosons, or heavy fermions. For example, calculations of one-loop flavor-changing interactions in the kaon system were able to successfully anticipate [1] the approximate value of the charm-quark mass. Similarly, some transitions in the B system (e.g., B^0-$\bar{B}^0$ mixing and the decay $B \to K l^+ l^-$) are especially sensitive [2] to the mass of the top quark. Often loop decays can also receive important contributions from physics beyond the SM (well-known [3] examples are $K \to \pi \nu \bar{\nu}$ and $B \to K^* \gamma$), which can give large enhancements or suppressions over the SM rates. In view of this, dedicated experimental facilities are being planned [4] for the study of rare K and B physics. The flavor-changing neutral-current (FCNC) transitions of a possible fourth-generation charged $-\frac{1}{3}$ b' quark have also been analyzed [5,6], where it was found that these FCNC decays could even dominate over the tree-level decays of the b' quark for certain values of the parameters. However, four-generation models (with light neutrinos) have been ruled out by the results [7] from the CERN e^+e^- collider LEP and from the SLAC Linear Collider (SLC) and will not be further discussed here.

Presently, the rare decays of every quark in the SM (and even some beyond the SM) have been thoroughly studied except for one, the top quark. Indeed, there are special reasons for studying rare decays of the t quark, as it is by far the largest fermion mass scale in the SM. As such, it might provide a unique window in the quest for new physics. Its rare decays (although anticipated to be small) should prove to be a useful quantitative reference point for comparing the SM to experiment. Also, at this mass scale, the effects of QCD should be unambiguous and presumably very small.

In this paper, we calculate the decays $t \to cV$, where $V=\gamma$, g, or Z, and $t \to cH$ in the SM, keeping all external as well as internal masses and momenta. We then study the possible effects of charged Higgs bosons on the transitions $t \to cV$ in the context of two-Higgs-doublet models. An exact calculation (to one-loop order) of the heavy-quark transition $q_i q_j \gamma$ (and subsequently $q_i q_j g$) in the SM has been performed by the authors of Ref. [8]; we have checked that our analytical expressions are in agreement with theirs. In Ref. [9], these results were used to study the process $t \to c\gamma$ for relatively light t quarks, $m_t \lesssim M_W$. Dutta Roy *et al.* [10] have also discussed the decay $t \to c\gamma$ in the SM in the limit of a very heavy m_t. Fritzsch [11] has estimated the rate for $t \to cZ$, and found that it could have a branching ratio of $\sim 10^{-4}$–10^{-2}. The present work complements and extends these previous results as it covers the t-quark-mass range $m_t > M_W$ and presents exact calculations for all the processes $t \to cV$ as well as $t \to cH$ in the SM and $t \to cV$ in two-Higgs-doublet models.

The Collider Detector at Fermilab (CDF) Collaboration has recently placed [12] a bound on the top-quark mass of $m_t > 89$ GeV, by searching for its semileptonic decay mode as predicted by the SM. A maximum-likelihood analysis [13], including full radiative corrections, of the recent data [7,12] on the properties of the W and Z bosons, has shown that $m_t < 200$ GeV at 95% C.L. and that the most likely value of m_t is ~ 135 GeV; these

bounds are in agreement with those obtained [14] from analyses of neutral-current data. Of course such bounds are only relevant to the SM; in extensions, such as extra Higgs doublets, the upper bound on m_t could be significantly different [15]. With future upgrades and increases in total integrated luminosity, experiments at the Fermilab Tevatron [16] expect to discover the top quark if its dominant decay modes are those of the SM and if its mass is in the range $m_t \lesssim 180$ GeV. The Superconducting Super Collider (SSC) will, of course, eventually produce a large number of t quarks, and may be able to observe rare top-quark interactions. There is also ongoing research for a linear e^+e^- collider with a center-of-mass energy in the range 500–1000 GeV. If such a machine materializes, it could become a unique facility for cleanly studying the physics of this mass scale [17].

The contents of this paper are as follows. In Sec. II we present our calculations and results in the SM for the processes $t\to c\gamma$, cg, and cZ. The transition $t\to cH$ is then examined for the SM in Sec. III. A brief overview of two-Higgs-doublet models and current restrictions on the parameters of the charged-Higgs-boson sector, as well as our results for the $H^{\pm}$ boson contributions to $t\to cV$, are presented in Sec. IV. Section V contains our conclusions and a brief discussion on the prospects of experimentally observing rare top-quark decays. Detailed formulas for heavy-quark FCNC transitions in both the SM and two-Higgs-doublet models are given in the Appendix.

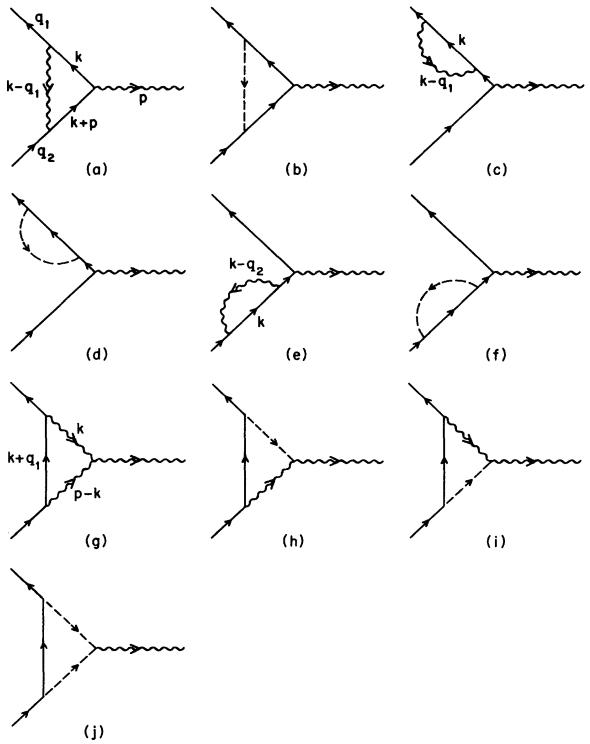

FIG. 1. Feynman diagrams responsible for the decay $t\to cV$. Solid lines represent quarks, wavy lines correspond to gauge bosons, and dashed lines are scalars.

II. $t\to cV$ IN THE STANDARD MODEL

In our calculation we use the 't Hooft–Feynman gauge (corresponding to $\xi=1$ in the R_ξ gauge) and take the external quarks t,c to be on shell. The ten Feynman diagrams responsible for the general tcV vertex in this gauge are displayed in Fig. 1. Our momenta conventions are as labeled in the figure. In calculating these diagrams we have kept all external and internal masses nonvanishing, and have assumed general left- and right-handed couplings which are tabulated in the Appendix for each possible elementary vertex. The $t\to cV$ transition matrix element is then generically given, for an internal quark i, by

$$M=V_{ci}V_{ti}^{\dagger}\bar{c}(q_1)[(a_1p^\mu+a_2q_2^\mu+a_3\gamma^\mu)L +(b_1p^\mu+b_2q_2^\mu+b_3\gamma^\mu)R\,]t(q_2)\epsilon_\mu(\lambda)\,, \tag{2.1}$$

where V_{ij} are the appropriate Kobayashi-Maskawa (KM) matrix elements [18], $L=(1-\gamma_5)/2$, and ϵ_μ is the polarization vector of the gauge boson V. The matrix element may be expressed in terms of the dipole transition via Gordon decomposition. The six form factors a_i and b_i are the sums of the contributions from each of the ten diagrams. They are functions of the masses and momenta of the external and internal quarks and gauge bosons, and contain n-dimensional integrals resulting from dimensional regularization. These integrals can be expressed in terms of Spence functions and in our calculations we follow the procedure and notation of Refs. [5,19]. The explicit expressions for the contributions from each diagram to the form factors are given in the Appendix.

In the case of $t\to c\gamma$ (and $t\to cg$) where the γ (or g) is on shell, electromagnetic current conservation implies the conditions

$$\begin{aligned}&\frac{\sqrt{x_t}}{2}a_2+b_3+\frac{\sqrt{x_c}}{2}b_2=0\,,\\ &\frac{\sqrt{x_c}}{2}a_2+a_3+\frac{\sqrt{x_t}}{2}b_2=0\,,\end{aligned} \tag{2.2}$$

with $x_i\equiv m_i^2/M_W^2$. We have checked that our results for the form factors obey these relations. For $V=Z$, the above expressions are proportional to M_Z^2 as required. We have also verified that the imaginary parts of our form factors display the proper analytic structure. As a final test of our work, we have calculated the partial widths for the corresponding FCNC decays of the fourth-generation b' quark and have confirmed that our numerical results agree with those of Ref. [6].

Once the form factors are determined, it is straightforward to calculate the decay widths. In the case of on-shell γ, or g emission ($q^2=0$), the width can be expressed as

$$\Gamma(t\to c\gamma,cg)=C_F\frac{\lambda^{1/2}(1,M_V^2/m_t^2,m_c^2/m_t^2)M_W^2}{32\pi m_t}$$
$$\times\{(x_t+x_c-M_V^2/M_W^2)[2(|f_3|^2+|h_3|^2)-x_t(|f_2|^2+|h_2|^2)$$
$$-2\sqrt{x_t}(\mathrm{Re}f_2\mathrm{Re}h_3+\mathrm{Im}f_2\mathrm{Im}h_3+\mathrm{Re}f_3\mathrm{Re}h_2+\mathrm{Im}f_3\mathrm{Im}h_2)]$$
$$-4\sqrt{x_cx_t}[\sqrt{x_t}(\mathrm{Re}f_2\mathrm{Re}f_3+\mathrm{Im}f_2\mathrm{Im}f_3+\mathrm{Re}h_2\mathrm{Re}h_3+\mathrm{Im}h_2\mathrm{Im}h_3)$$
$$+x_t(\mathrm{Re}f_2\mathrm{Re}h_2+\mathrm{Im}f_2\mathrm{Im}h_2)+4(\mathrm{Re}f_3\mathrm{Re}h_3+\mathrm{Im}f_3\mathrm{Im}h_3)]\}\ , \tag{2.3}$$

with C_F being a color factor given by $C_F=1$ $(\frac{4}{3})$ for the γ (g), M_V is the vector-boson mass, which we keep for use in Eq. (2.5) ($M_V=0$ in the case of $V=\gamma,g$), and $\lambda(a,b,c)=a^2+b^2+c^2-2(ab+ac+bc)$ is the usual triangle function. f and h explicitly demonstrate the Glashow-Iliopoulos-Maiani (GIM) mechanism [20] and are given by

$$f_i=\sum_{j=b,s}V_{cj}V_{tj}^{\dagger}[a_i(x_M=x_j)-a_i(x_M=x_d)]\ ,$$
$$h_i=\sum_{j=b,s}V_{cj}V_{tj}^{\dagger}[b_i(x_M=x_j)-b_i(x_M=x_d)]\ , \tag{2.4}$$

where M represents the internal quarks d, s, or b, and a_i,b_i are the form factors summed over the ten contributing diagrams. The partial width for $t\to cZ$ is

$$\Gamma(t\to cZ)=\Gamma(t\to c\gamma)+\frac{\lambda^{1/2}(1,M_Z^2/m_t^2,m_c^2/m_t^2)M_W^4}{16\pi m_tM_Z^2}$$
$$\times\Big[(|f_2|^2+|h_2|^2)(\hat{q}_1\cdot\hat{q}_2)(\hat{q}_2\cdot\hat{p})^2+(|f_3|^2+|h_3|^2)[2(\hat{q}_1\cdot\hat{p})(\hat{q}_2\cdot\hat{p})-M_Z^2/M_W^2(\hat{q}_1\cdot\hat{q}_2)]$$
$$+2(\mathrm{Re}f_2\mathrm{Re}h_3+\mathrm{Im}f_2\mathrm{Im}h_3+\mathrm{Re}f_3\mathrm{Re}h_2+\mathrm{Im}f_3\mathrm{Im}h_2)\sqrt{x_t}(\hat{q}_1\cdot\hat{p})(\hat{q}_2\cdot\hat{p})$$
$$+2(\mathrm{Re}f_2\mathrm{Re}f_3+\mathrm{Im}f_2\mathrm{Im}f_3+\mathrm{Re}h_2\mathrm{Re}h_3+\mathrm{Im}h_2\mathrm{Im}h_3)\sqrt{x_c}(\hat{q}_2\cdot\hat{p})^2$$
$$+2(\mathrm{Re}f_3\mathrm{Re}h_3+\mathrm{Im}f_3\mathrm{Im}h_3)\sqrt{x_cx_t}\frac{M_Z^2}{M_W^2}+2(\mathrm{Re}f_2\mathrm{Re}h_2+\mathrm{Im}f_2\mathrm{Im}h_2)\sqrt{x_cx_t}(\hat{q}_2\cdot\hat{p})^2\Big], \tag{2.5}$$

f_i,h_i are as given in Eq. (2.4), the dot products are in the Appendix, all momenta are scaled by the W-boson mass, $\hat{p}$ $(\hat{q}_i)\equiv p/M_W$ (q_i/M_W), and $\Gamma(t\to c\gamma)$ is given in Eq. (2.3) with $M_V=M_Z$ in this case.

We compute the branching ratio for $t\to cV$ by taking the SM charged-current two-body decay $t\to bW$ (where the W is real for top quarks satisfying the CDF limit $m_t>89$ GeV) to be the dominant t-quark decay mode. The partial width for this two-body tree-level process is straightforward to calculate [21], and as expected, is quite large with a value of $\Gamma(t\to bW)=90$ MeV (2.5 GeV) for $m_t=90$ (200) GeV. We will then approximate the branching ratio for $t\to cV$ by

$$B(t\to cV)=\frac{\Gamma(t\to cV)}{\Gamma(t\to bW)}\ . \tag{2.6}$$

In our numerical calculations, we take the central value of the allowed range for the appropriate KM matrix elements as given in Ref. [22], the value of the Z-boson mass as measured [7] at CERN LEP $M_Z=91.177$ GeV, the W-boson mass as determined [12] by the Collider Detector at Fermilab (CDF) and UA2 Collaborations $M_W=80.10$ GeV, $\sin^2\theta_W=0.23$, $\alpha_{\mathrm{em}}=1/128.8$, $\alpha_s=1.4675/\ln(m_t^2/\Lambda_{\mathrm{QCD}}^2)$ with $\Lambda_{\mathrm{QCD}}=180$ MeV, and the following values for the quark masses: $m_d=10$ MeV, $m_s=150$ MeV, $m_c=1.5$ GeV, and $m_b=5.0$ GeV. We take the top quark to lie in the range $89<m_t<200$ GeV.

Our results for $B(t\to cV)$ as a function of m_t are presented in Fig. 2, where the dashed, solid, and dashed-dotted curves correspond to $B(t\to cg)$, $B(t\to c\gamma)$, and

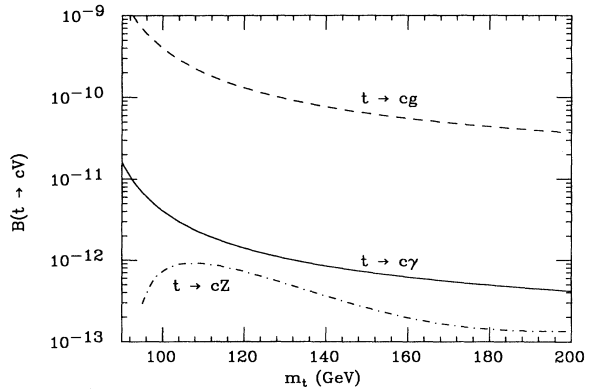

FIG. 2. $B(t\to cV)$ as a function of m_t in the SM. The dashed curve denotes the process $t\to cg$, the solid curve $t\to c\gamma$, and the dashed-dotted curve $t\to cZ$.

$B(t\to cZ)$, respectively. The process $t\to cg$ has the largest branching fraction with $B(t\to cg)\sim 10^{-10}$ for $m_t \gtrsim 110$ GeV, and for $m_t \sim 90$ GeV $B(t\to cg)$ rises to $\sim 10^{-9}$. $t\to c\gamma$ and $t\to cZ$ occur at much smaller rates of $\sim 10^{-13}-10^{-12}$. It is clear that the loop decays of the t quark are very small in the SM. This is due to a strong GIM suppression from the small values of the internal quark masses $m_{b,s,d}$, as well as the large tree-level rate for $t\to bW$.

QCD corrections have been found [2] to give large enhancements to the rate for the process $b\to s\gamma$ and one might wonder if this could also occur in the case of rare t-quark decays. In the B-meson system, the leading QCD corrections are calculated by integrating from the electroweak scale down to m_b in the leading-log approximation. This produces a large shift in the amplitude and softens the GIM power suppression to a log suppression. However, in the t-quark system, m_t is already of order of the electroweak scale so the integration procedure will not produce such large logarithms and hence the QCD corrections of this type should be small.

III. $t\to cH$ IN THE STANDARD MODEL

The decay $t\to cH$ proceeds through the same ten Feynman diagrams that mediate the process $t\to cV$ (which are displayed in Fig. 1), except in this case the external vector boson V is replaced by an external scalar H. The general vertex for the on-shell $t\to cH$ decay is

$$M = V_{ci}V_{ti}^{\dagger}\bar{c}(q_1)(\alpha L+\beta R)t(q_2)\ , \tag{3.1}$$

where α and β represent the sum of the contributions from all ten diagrams. These contributions have been calculated in Ref. [5] for the case of the fourth-generation quark decay $b'\to bH$, where the masses and momenta of all external and internal particles have been kept. The expressions for α and β are given explicitly in the Appendix of this reference and will not be reproduced here. The partial width for $t\to cH$ can then be written as

$$\Gamma(t\to cH)=\frac{M_W}{32\pi x_t^{3/2}}\sqrt{(x_c+x_t-x_H)^2-4x_cx_t}\times[(|f|^2+|h|^2)(x_c+x_t-x_H)+4(\mathrm{Re}f\,\mathrm{Re}h+\mathrm{Im}f\,\mathrm{Im}h)\sqrt{x_cx_t}]\ , \tag{3.2}$$

with $x_H=M_H^2/M_W^2$ and f,h exhibit the GIM mechanism for α and β as given in Eq. (2.4) with $a_i\to\alpha$ and $b_i\to\beta$.

The branching ratio is computed as in the preceding section and $B(t\to cH)$ is displayed in Fig. 3 as a function of m_t for various values of the Higgs-boson mass that are consistent with the LEP limit [7] of $m_H \gtrsim 42$ GeV. Note that for a given m_H, the branching fraction clearly increases as the value of m_t increases (for $m_t \gtrsim 100$ GeV), giving maximum values of $B(t\to cH)\sim 10^{-7}$ for $m_t<200$ GeV. The branching fractions generally lie in the range 10^{-8}–10^{-7} for all values of m_t and m_H, once the severe reduction in phase space has been overcome. Comparing these results with those in Fig. 2 we see that generally

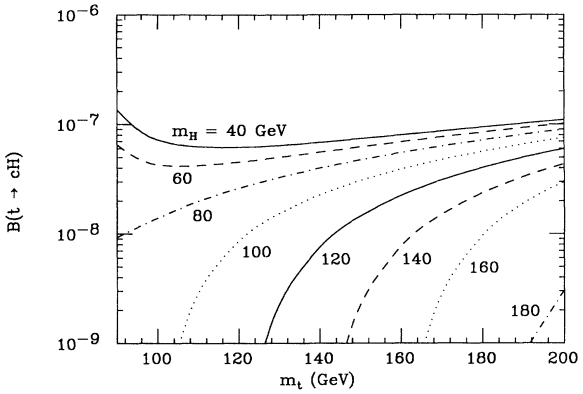

FIG. 3. $B(t\to cH)$ as a function of m_t in the SM for the various values of m_H as indicated.

$B(t\to cH)>B(t\to cV)$. This is due to a softening of the GIM suppression in this case as the Higgs-boson–quark coupling is proportional to the quark mass.

IV. $t\to cV$ IN THE TWO-HIGGS-DOUBLET MODEL

Since we have seen that the branching ratios for rare top-quark decays in the SM are small, perhaps new physics can significantly increase the rates for these decays and make them observable. In order to quantify the effects that new physics could have on rare t-quark decays, we examine the processes $t\to cV$ in two-Higgs-doublet models. An enlarged Higgs sector is a relatively simple extension of the SM and naturally occurs in many theories, such as supersymmetry, models with spontaneous CP violation, and some grand unified theories (e.g., E_6). The existence of two (or more) Higgs doublets necessitates the presence of charged Higgs bosons which influence one-loop processes.

We consider two distinct two-Higgs-doublet models which naturally avoid tree-level FCNC [23]. In model I, one doublet (ϕ_2) gives masses to all fermions and the other doublet (ϕ_1) essentially decouples from the fermions. In a second model (model II) ϕ_2 gives mass to the up-type quarks, while the down-type quarks and charged leptons receive a mass from ϕ_1. Each doublet obtains a vacuum expectation value (VEV) v_i subject only to the constraint that $v_1^2+v_2^2=v^2$, where v is the usual VEV of the SM. The generic charged-Higgs-boson coupling to fermions (assuming massless neutrinos) in both models is given by

$$\mathcal{L}=\frac{g}{2\sqrt{2}M_W}H^{\pm}[V_{ij}m_{u_i}F_u\bar{u}_i(1-\gamma_5)d_j+V_{ij}m_{d_j}F_d\bar{u}_i(1+\gamma_5)d_j+m_lF_l\bar{\nu}(1+\gamma_5)l]+\mathrm{H.c.}\ , \tag{4.1}$$

where g is the usual $SU(2)_L$ coupling constant. In model I, $F_u=\cot\beta$ and $F_d=F_l=-\cot\beta$ and in model II, $F_u=\cot\beta$ and $F_d=F_l=\tan\beta$, where $\tan\beta\equiv v_2/v_1$ is the ratio of VEV's; this is summarized in Table I. Model II is that which is present in supersymmetry and E_6 theories. The mass $m_{H^{\pm}}$ and the ratio v_2/v_1 are *a priori* free pa-

TABLE I. Summary of which doublet, ϕ_1 or ϕ_2, gives mass to each quark type and the values of the coefficients F_f ($f=u,d$) in the charged-Higgs-boson Lagrangian in Eq. (4.1) for models I and II.

	Model I		Model II	
f	VEV	F_f	VEV	F_f
u	2	$\cot\beta$	2	$\cot\beta$
d	2	$-\cot\beta$	1	$\tan\beta$

rameters in general two-Higgs-doublet models. The current experimental bound from LEP [7] on the $H^\pm$ mass is $m_{H^\pm} > 35.4$ (43.0) GeV at 95% C.L. with $B(H^\pm \to cs(\tau\nu)) = 100\%$.

Semiquantitative restrictions on $m_{H^\pm}$ and $\tan\beta$ can be set by requiring that the $H^\pm$ width not be too large and that the $\bar{t}bH$ coupling remain perturbative. It is clear from Eq. (4.1) that the width and $\bar{t}bH$ coupling both grow rapidly with increasing m_t and decreasing $\tan\beta$, and hence perturbation theory may become endangered for some values of the parameters. This is illustrated in Fig. 4, which shows the total width of the t quark for $m_t > m_b + m_{H^\pm}$ as a function of $\tan\beta$ with $m_{H^\pm} = 50$ GeV and $m_t = 100$, 150, and 200 GeV. If we demand that the theory remain perturbative, a bound on $\tan\beta$ as a function of m_t is obtained. By taking Γ_t/m_t (or $\Gamma_{H^\pm}/m_{H^\pm}$) $< \frac{1}{2}$ and also requiring that the $\bar{t}bH$ coupling be smaller than the QCD coupling $g_s^2 = 4\pi\alpha_s(M_W^2)$ as definitions of the perturbative region, the bound $\tan\beta \lesssim m_t/(600\text{ GeV})$ is obtained. This restriction applies in both models. In model II there is a corresponding upper limit on $\tan\beta$ of $\cot\beta \lesssim m_b/(600\text{ GeV})$, which arises from the term proportional to $m_b V_{tb}\tan\beta$ in Eq. (4.1).

Further restrictions on the parameters contained in two-Higgs-doublet models can be obtained from an analysis of possible charged-Higgs-boson contributions to low-energy data. Such contributions to B_d^0-$\bar{B}_d^0$ and D^0-$\bar{D}^0$ mixing, ϵ, the $K_L - K_S$ mass difference, and ϵ'/ϵ have been examined in Ref. [24], where the overall region which is consistent with current experimental measurements has been determined. The results are essentially equivalent in both models I and II, and are found to be roughly given by the above perturbation bound, $\tan\beta \gtrsim m_t/600$ GeV. Additional constraints can be obtained if $H^\pm$ contributions to the decay $b \to s\gamma$ are considered [3,24]; however, these limits rely heavily on the precise value of the ratio of exclusive to inclusive rates.

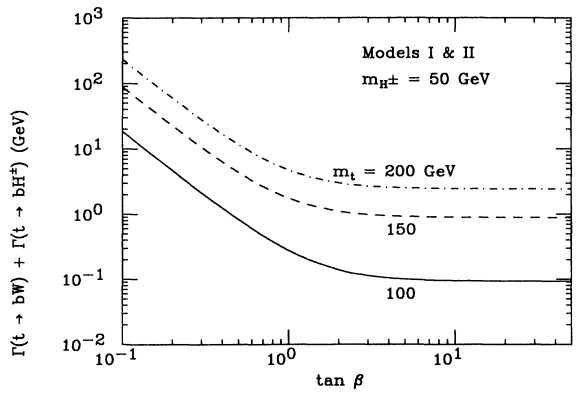

FIG. 4. The total width of the t quark, $\Gamma(t \to bW) + \Gamma(t \to bH^\pm)$, as a function of $\tan\beta$ for $m_t = 100$, 150, and 200 GeV corresponding to the solid, dashed, and dashed-dotted curves, respectively.

Charged Higgs bosons can contribute to the processes $t \to cV$ via the Feynman diagrams of Figs. 1(b), 1(d), 1(f), and 1(j), with the unphysical scaler ϕ being replaced by $H^\pm$. The transition matrix element and the expressions for the partial widths have exactly the same form as in Eqs. (2.1), (2.3), and (2.5). The six form factors are now a sum of the contributions from the ten SM diagrams and the four $H^\pm$ diagrams and are a function of the quark and gauge boson masses and momenta as well as $m_{H^\pm}$ and $\tan\beta$. The precise expressions for the $H^\pm$ contributions to the form factors are listed in the Appendix. We have verified that our current-conservation conditions of Eq. (2.2) are still satisfied in these models, and that our expressions for the charged-Higgs-boson diagrams 1(b), 1(d), 1(f), and 1(j) approach those of the SM when the $H^\pm$ couplings approach those of the unphysical scalar ϕ.

Our results for the branching fractions for $t \to c\gamma$, $t \to cg$, and $t \to cZ$ as a function of $\tan\beta$ are presented in Figs. 5, 6, and 7, respectively. We show results for model I with $m_t = 100$ GeV and $m_t = 200$ GeV, and model II with $m_t = 100$ and 200 GeV, corresponding to the figure labels (a), (b), (c), and (d), respectively. In each figure, the solid curve represents $m_{H^\pm} = 50$ GeV, the dashed $m_{H^\pm} = 100$ GeV, the dotted $m_{H^\pm} = 250$ GeV, and the dashed-dotted $m_{H^\pm} = 500$ GeV. Note that when the decay $t \to bH^\pm$ is kinematically allowed, the charged-Higgs-boson contributions to the one-loop induced flavor-changing transitions are slightly suppressed for some values of $\tan\beta$.

In model I, enhancements over the SM rates of up to three orders of magnitude are obtainable [$B(t \to cg) \sim 10^{-6}$ for m_t, $m_{H^\pm} = 100$ GeV] for small values of $\tan\beta$ ($\lesssim 0.5$), while for larger values of $\tan\beta$ ($\gtrsim 2$) the branching fraction approaches its SM value. This behavior obviously reflects the $H^\pm$ fermion couplings, which are all proportional to $\cot\beta$ in this model. However, recall that the perturbative and low-energy bounds restrict $\tan\beta \gtrsim 0.167$ (0.333) for $m_t = 100$ (200) GeV, and thus the ranges of $\tan\beta$ which yield the largest enhancements are those which have been ruled out above.

The situation is somewhat different in the case of model II. Slight enhancements are possible for small values of $\tan\beta$ (up to one order of magnitude), but the biggest increases in rate (up to 3–4 orders of magnitude) are obtained when $\tan\beta$ takes on larger values, $\tan\beta \gtrsim 5$–10. For example, with $m_t = 100$ GeV, $m_{H^\pm} = 100$ GeV, and $\tan\beta = 50$, $B(t \to cg) \sim 2 \times 10^{-6}$. These large enhancements occur when $\tan\beta$ is large enough to make the $m_b\tan\beta$ term in the charged Higgs Lagrangian dominant.

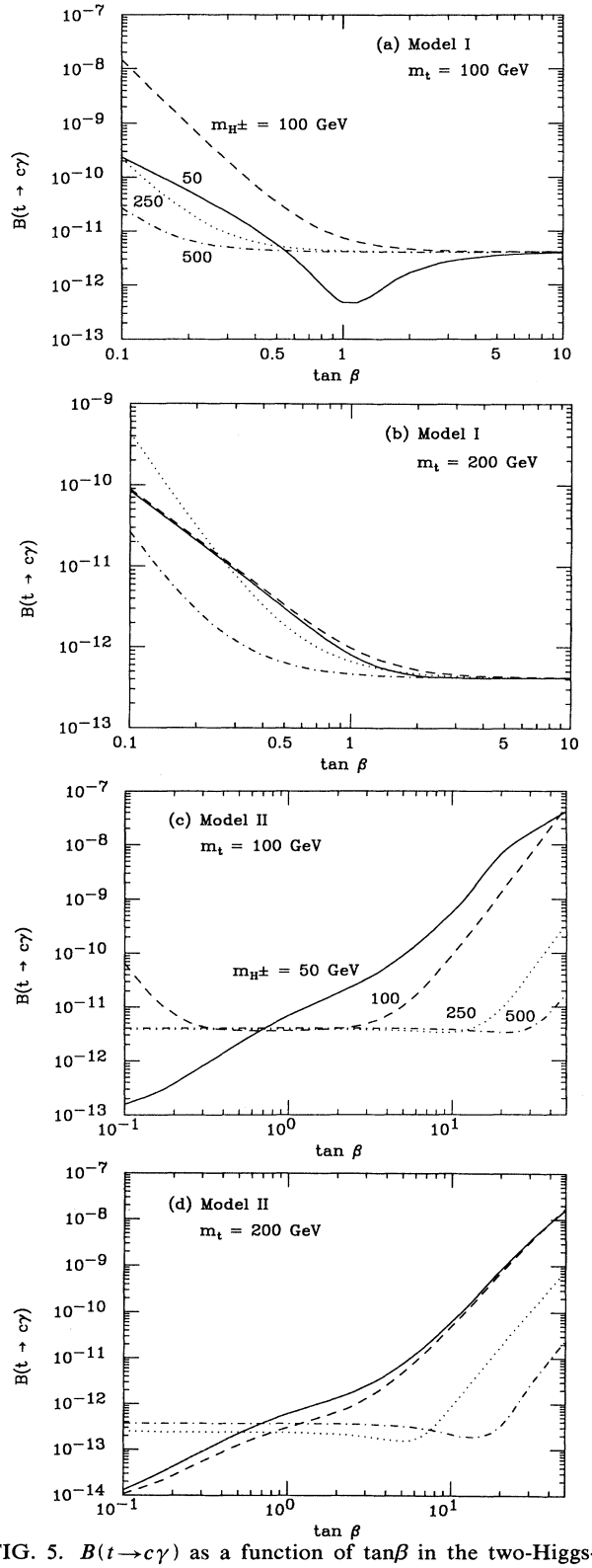

FIG. 5. $B(t\to c\gamma)$ as a function of tanβ in the two-Higgs-doublet model with (a) $m_t=100$ GeV in model I, (b) $m_t=200$ GeV in model I, (c) $m_t=100$ GeV in model II, (d) $m_t=200$ GeV in model II. The solid curve represents $m_{H^\pm}=50$ GeV, dashed $m_{H^\pm}=100$ GeV, dotted $m_{H^\pm}=250$ GeV, and dashed-dotted $m_{H^\pm}=500$ GeV.

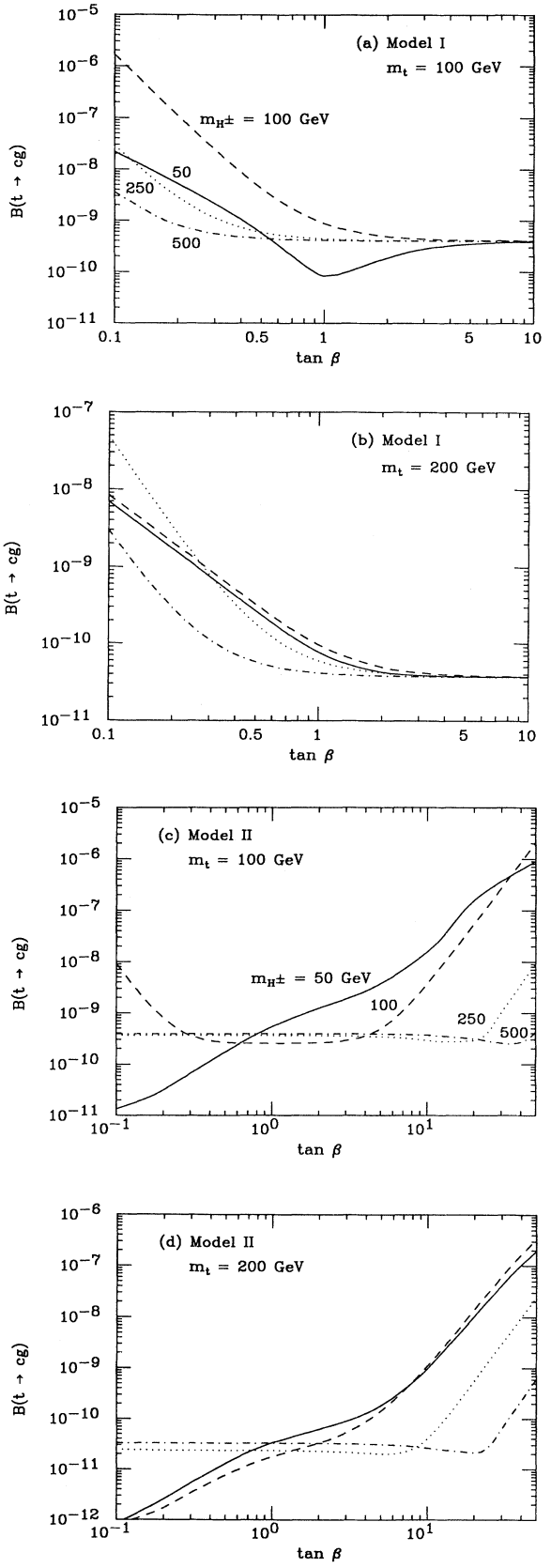

FIG. 6. Same as in Fig. 5, except for the decay $t\to cg$.

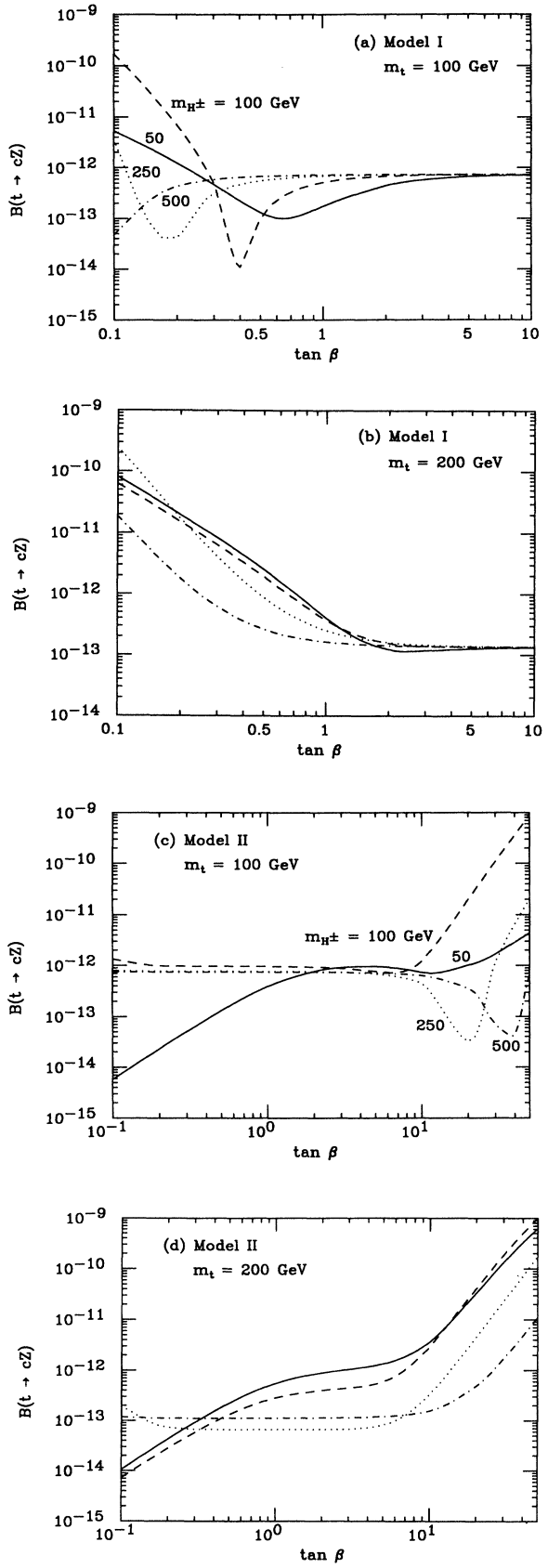

FIG. 7. Same as in Fig. 5, except for the decay $t \to cZ$.

This region where $\tan\beta$ takes on large values is not ruled out by experiment and is predicted [25] to occur in some grand unified theories.

Figure 8 shows the branching fraction for (a) $t \to c\gamma$, (b) $t \to cg$, and (c) $t \to cZ$ as a function of m_t with $m_{H^\pm} = 100$ GeV in model I with $\tan\beta = 0.25$ and 1.0 (corresponding to the dashed and solid curves, respectively) and in model II with $\tan\beta = 0.25$ and 20.0 (represented by the dotted and dashed-dotted curves, respectively). Here one can see the general trend for enhancements in model I (II) for smaller (larger) values of $\tan\beta$ [e.g.,

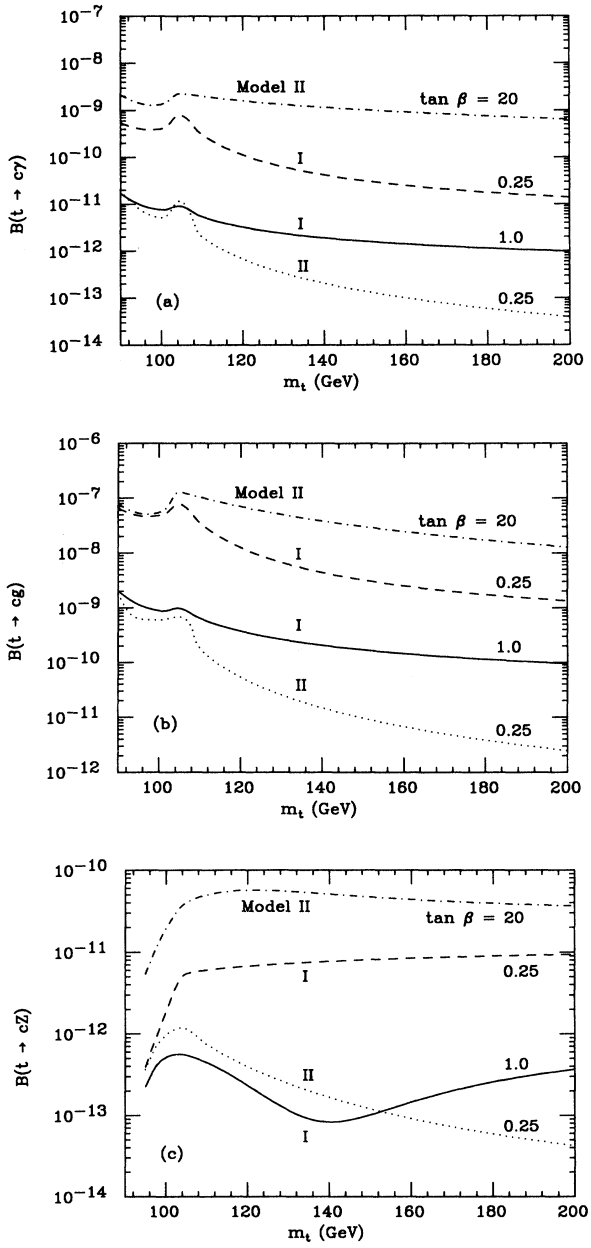

FIG. 8. (a) $B(t \to c\gamma)$, (b) $B(t \to cg)$, and (c) $B(t \to cZ)$ as a function of m_t with $m_{H^\pm} = 100$ GeV in model II with $\tan\beta = 20$ (dashed-cotted), model II with $\tan\beta = 0.25$ (dotted), model I with $\tan\beta = 1.0$ (solid), and model I with $\tan\beta = 0.25$ (dashed).

$B(t\to cg)\sim 10^{-8}$–10^{-7} in model II with $\tan\beta=20$]. The increase in the branching fraction due to the anomalous threshold behavior at $m_t=m_b+m_{H^\pm}$ is also demonstrated.

V. CONCLUSIONS

In summary, we have calculated and presented expressions for the flavor-changing transitions $t\to c\gamma$, cg, cZ, and cH in the SM, keeping all masses and momenta nonvanishing. We found the branching fractions for these decays to be small in the SM, and are of order $B(t\to c\gamma)\sim 10^{-12}$, $B(t\to cg)\sim 10^{-10}$, $B(t\to cZ)\sim 10^{-13}$–10^{-12}, and $B(t\to cH)\sim 10^{-8}$–10^{-7} for $90<m_t<200$ GeV. The fact that these decay rates are so small in the SM (and are relatively free of QCD and hadronic uncertainties) can, in principle, provide a test for possible new physics. In practice, backgrounds from other SM processes can be a serious problem and detailed studies will have to be carried out before any claims can be made. If one of these processes were observed at a larger rate than given above, and could not be accounted for by SM background processes, then it could be a signal for new interactions. Along this vein, we have extended our study to include contributions from charged Higgs bosons present in two-Higgs-doublet models. We found that large enhancements of the SM rates are possible for various values of the parameters, giving the overall maximum values of the branching fractions to be $B(t\to c\gamma)\sim 10^{-8}$, $B(t\to cg)\sim 10^{-6}$, and $B(t\to cZ)\sim 10^{-9}$. Further studies of these decays in models beyond the SM should be made in order to determine if even larger increases in the rates are possible. The rate for the three-body decay, $t\to cq\bar{q}$, through virtual gluons, and for CP violation in t decays should also be examined [26] to provide a benchmark for SM predictions.

The SSC can be expected to produce a large number of t quarks; the predicted event rate [21] is roughly 3.5×10^8, 1.2×10^8 and 5.6×10^7 $t\bar{t}$ pairs per year for $m_t=110$, 150, and 180 GeV, respectively, assuming an integrated luminosity of 10^4 pb^{-1} per year. Even with 100% acceptance and tagging efficiencies, the SSC detectors will not observe these rare top-quark decays in the SM, unless there is a substantial increase in luminosity. We have shown that in models with an extended Higgs sector the event rates can be enhanced, e.g., $t\to cg$ could occur at a rate of $\sim 10^{-6}$ (with favorable values of the parameters), and thus may be observable with efficient t-quark tagging. A high-energy linear e^+e^- collider could, in principle, be the ideal place to study these rare decays, as t-quark events can be cleanly separated by tagging the isolated lepton from the top semileptonic decay. However, a high integrated luminosity would have to be achieved before observation of these rare decay modes becomes feasible.

Clearly, before one can use our calculations in the context of interpretation of experimental searches for these rare decays, issues related to experimental backgrounds are very important and will have to be dealt with, but are beyond the scope of this work. For illustration, the decay $t\to cH$ has a potential background from multibody reactions such as $t\to HbW$, followed by the hadronic decay of the real or virtual W [27]. The branching fraction for this multibody process is presented in Ref. [28]. For the case of real W emission, i.e., $m_t>M_W+m_b+m_H$, these authors find $B=\Gamma(t\to HbW)/\Gamma(t\to bW)\simeq 10^{-5}$, few $\times 10^{-4}$ for $m_t=200$ GeV and $m_H=100$, 50 GeV, respectively. Scaling this by the hadronic branching fraction of the W (so that the final state W is more difficult to identify), we see that this multibody background can be larger than the SM rate for $t\to cH$ by 2–3 orders of magnitude. For the case of virtual W emission, the branching fraction for $t\to HbW^*\to Hbqq'$, is much smaller than in the case of real W's. In either case, this background can be substantially reduced by using appropriate experimental cuts. For instance, in the process $t\to cH\to cb\bar{b}$, the charm-quark jet will have a very large transverse momentum (recall $m_H>45$ GeV from LEP [7]) and the invariant mass of the recoil $b\bar{b}$ jets should add up to the Higgs-boson mass. Thus, an examination of the recoil invariant mass of top-quark events, which contain a jet with large p_T, should discard most, if not all, of these types of backgrounds [29]. Detailed Monte Carlo studies clearly should be done for these processes and their potential backgrounds, but only after the specific characteristics of the actual detectors, e.g., acceptances, efficiencies, cracks, etc., become known.

The topic of rare top-quark physics has just begun to be explored and may yield some surprises, both theoretical and experimental.

ACKNOWLEDGMENTS

We would like to thank W.-Y. Keung and T. Rizzo for useful conversations and V. Barger and R. Willey for discussions of potential backgrounds to these rare decay modes. The research of G.E. has been supported in part by the fund for Promotion of Research at the Technion and by the Technion V.P.R. Fund and G. S. Elkin Research Fund. The research of J.L.H. was supported in part by the University of Wisconsin Research Committee with funds granted by the Wisconsin Alumni Research Foundation and in part by the U.S. Department of Energy under Contract No. DE-AC02-76ER00881.

APPENDIX: RELEVANT FORMULAS

Here we present the expressions, keeping all masses and momenta, for the form factors for each of the diagrams in Fig. 1. In the following A^μ–J^μ denote results for the diagrams labeled (a)–(j) in Fig. 1 for an internal quark with mass M. B_0, B_1, C_0, $\tilde{C}_0$, and C_{ij} represent the scalar functions in the notation of Refs. [5,19], and for each diagram are functions of the masses and momenta as given. All masses and momenta are scaled by the W-boson mass M_W (e.g., $x_i\equiv m_i^2/M_W^2$, $\hat{M}_W^2\equiv M_W^2/M_W^2$, $\hat{p}^2\equiv p^2/M_W^2$), g is the usual $SU(2)_L$ weak coupling constant, $\epsilon=n-4$ (where n represents the number of dimensions in the dimensional-regularization procedure), $R=(1+\gamma_5)/2$, and the values of the coefficients A_j, B_j, C, D, and E ($j=u,d$ for quarks with weak isospin of $\frac{1}{2}$, $-\frac{1}{2}$, respectively) are given in Table II:

TABLE II. Values of the coefficients in Eqs. (A1)–(A10). $\hat{M}_W \equiv M_W/M_W$, c_W (s_W)$=\cos\theta_W$ ($\sin\theta_W$), where θ_W is the weak mixing angle, $x_W=\sin^2\theta_W$, g (g_s) represents the usual weak (strong) coupling constant, and $e=|e|$ is the electric charge of the proton.

V	A_u	A_d	B_u	B_d	C	D	E
γ	$\frac{2}{3}e$	$-\frac{1}{3}e$	$\frac{2}{3}e$	$-\frac{1}{3}e$	e	$gs_W\hat{M}_W$	e
g	g_s	g_s	g_s	g_s	0	0	0
Z	$\frac{g}{2c_W}(1-\frac{4}{3}x_W)$	$\frac{g}{2c_W}(-1+\frac{2}{3}x_W)$	$\frac{-g}{2c_W}\frac{4}{3}x_W$	$\frac{g}{2c_W}\frac{2}{3}x_W$	gc_W	$\frac{-gx_W\hat{M}_W}{c_W}$	$\frac{g}{2c_W}(c_W^2-s_W^2)$

$$
\begin{aligned}
A^\mu=\frac{g^2}{2}(&-2\sqrt{x_c}(\epsilon-2)A_d(C_{11}+C_{21})p^\mu L+2\sqrt{x_c}A_d[\epsilon C_{12}+(\epsilon-2)C_{23}]q_2^\mu L\\
&+\{A_d[(-2x_t+\epsilon\hat{p}^2-\epsilon x_c)C_{12}+(\epsilon-2)(2C_{24}-\tilde{C}_0-\hat{p}^2C_{11})]+(\epsilon-2)x_M B_d C_0\}\gamma^\mu L\\
&+2\sqrt{x_t}A_d[(\epsilon-2)(C_{11}-C_{23}+C_{21})-\epsilon C_{12}]p^\mu R+2\sqrt{x_t}A_d[2C_{12}+(\epsilon-2)(C_{22}-C_{23})]q_2^\mu R\\
&-\sqrt{x_c x_t}A_d(\epsilon+2)C_{12}\gamma^\mu R)\ ,
\end{aligned}
\tag{A1}
$$

with $C_{ij}(\hat{p},-\hat{q}_2,\sqrt{x_M},\sqrt{x_M},\hat{M}_W)$,

$$
\begin{aligned}
B^\mu=\frac{g^2}{2\hat{M}_W^2}(&[2x_t\sqrt{x_c}A_d(C_{12}+C_{23}-C_{11}-C_{21})+2x_M\sqrt{x_c}B_d(C_0+2C_{11}+C_{21})]p^\mu L\\
&+\{2\sqrt{x_c}A_d[x_t(C_{23}-C_{22})+x_M(C_{11}-C_{12})]-2x_M\sqrt{x_c}B_d(C_0+C_{11}+C_{12}+C_{23})\}q_2^\mu L\\
&+\{x_M A_d[x_t(C_0+C_{11}-C_{12})-x_c C_{11}-x_M C_0]+x_M B_d[x_c(C_0+C_{11})+x_t(-C_{11}+C_{12})]\\
&\quad+A_d x_c x_t C_{12}+x_M B_d[\tilde{C}_0+\hat{p}^2C_{11}+(x_c-\hat{p}^2)C_{12}-2C_{24}]\}\gamma^\mu L\\
&+\{2\sqrt{x_t}A_d[x_M(C_0+C_{11})+x_c(C_{11}+C_{21})]+2x_M\sqrt{x_t}B_d(C_{12}-C_{11}-C_{21}+C_{23})\}p^\mu R\\
&+\{-2\sqrt{x_t}A_d[x_M(C_0+C_{11})+x_c(C_{12}+C_{23})]+2x_M\sqrt{x_t}B_d(C_{11}-C_{12}-C_{22}+C_{23})\}q_2^\mu R\\
&+\sqrt{x_c x_t}A_d[x_M(C_0+C_{12})+\hat{p}^2C_{11}+(x_c-\hat{p}^2)C_{12}+\tilde{C}_0-2C_{24}]\gamma^\mu R)\ ,
\end{aligned}
\tag{A2}
$$

with $C_{ij}(\hat{p},-\hat{q}_2,\sqrt{x_M},\sqrt{x_M},\hat{M}_W)$,

$$
C^\mu=\frac{g^2(\epsilon-2)}{2(x_t-x_c)}(x_c A_u B_1\gamma^\mu L+\sqrt{x_c x_t}B_u B_1\gamma^\mu R)\ ,
\tag{A3}
$$

with $B_1(-\hat{q}_1,\sqrt{x_M},\sqrt{x_M},\hat{M}_W)$,

$$
D^\mu=\frac{g^2}{2\hat{M}_W^2(x_c-x_t)}\{[x_c(x_t+x_M)A_u B_1+x_M(x_c+x_t)A_u B_0]\gamma^\mu L+\sqrt{x_c x_t}[(x_M+x_c)B_u B_1+2x_M B_u B_0]\gamma^\mu R\}\ ,
\tag{A4}
$$

with $B_i(-\hat{q}_1,\sqrt{x_M},\hat{M}_W)$,

$$
E^\mu=\frac{g^2(\epsilon-2)}{2(x_c-x_t)}(x_t A_u B_1\gamma^\mu L+\sqrt{x_c x_t}B_u B_1\gamma^\mu R)\ ,
\tag{A5}
$$

with $B_1(-\hat{q}_2,\sqrt{x_M},\hat{M}_W)$,

$$
F^\mu=\frac{g^2}{2\hat{M}_W^2(x_t-x_c)}\{[x_t(x_c+x_M)A_u B_1+x_M(x_c+x_t)A_u B_0]\gamma^\mu L+\sqrt{x_c x_t}[(x_M+x_t)B_u B_1+2x_M B_u B_0]\gamma^\mu R\}\ ,
\tag{A6}
$$

with $B_i(-\hat{q}_2\sqrt{x_M},\hat{M}_W)$,

$$
\begin{aligned}
G^\mu=\frac{g^2C}{2}\{&(\epsilon-2)\sqrt{x_c}(C_0+3C_{11}+2C_{21})p^\mu L+2\sqrt{x_c}[2C_0+C_{11}+C_{12}-(\epsilon-2)(C_{12}+C_{23})]q_2^\mu L\\
&+[x_c(C_{11}-C_0)-x_t(2C_0+C_{11}+C_{12})+2\hat{p}^2(C_0+C_{11})+2\tilde{C}_0-2(\epsilon-2)C_{24}]\gamma^\mu L\\
&+\sqrt{x_t}[2C_{11}-2C_0-4C_{12}-(\epsilon-2)(C_{11}-C_{12}+2C_{21}-2C_{23})]p^\mu R\\
&+2\sqrt{x_t}[C_0-C_{11}+2C_{12}+(\epsilon-2)(C_{23}-C_{22})]q_2^\mu R-3\sqrt{x_c x_t}(C_0+C_{12})\gamma^\mu R\}\ ,
\end{aligned}
\tag{A7}
$$

with $C_{ij}(-\hat{p},\hat{q}_2,\hat{M}_W,\hat{M}_W,\sqrt{x_M})$,

$$H^\mu=\frac{g^2D}{2\hat{M}_W}\{2\sqrt{x_c}(C_{12}-C_{11})q_2^\mu L+[(x_c-x_M)C_0+x_cC_{11}]\gamma^\mu L+\sqrt{x_cx_t}(C_{11}-C_{12})\gamma^\mu R\}\ , \tag{A8}$$

with $C_{ij}(-\hat{p},\hat{q}_2,\hat{M}_W,\hat{M}_W,\sqrt{x_M})$,

$$I^\mu=\frac{g^2D}{2\hat{M}_W}\{[x_t(C_{12}-C_{11})-x_MC_0]\gamma^\mu L-2\sqrt{x_t}(C_0+C_{11})(p^\mu R-q_2^\mu R)-\sqrt{x_cx_t}(C_0+C_{11})\gamma^\mu R\}\ , \tag{A9}$$

with $C_{ij}(-\hat{p},\hat{q}_2,\hat{M}_W,\hat{M}_W,\sqrt{x_M})$,

$$\begin{aligned}J^\mu=\frac{g^2E}{2\hat{M}_W^2}\{&\sqrt{x_c}[x_t(C_{11}-C_{12}+2C_{21}-2C_{23})-x_M(C_{11}+2C_{21})]p^\mu L+2\sqrt{x_c}[x_t(C_{22}-C_{23})+x_MC_{23}]q_2^\mu L\\&+2x_MC_{24}\gamma^\mu L+\sqrt{x_t}[-x_c(C_0+3C_{11}+2C_{21})+x_M(C_0+3C_{11}-C_{12}+2C_{21}-2C_{23})]p^\mu R\\&+2\sqrt{x_t}[x_c(C_{12}+C_{23})+x_M(C_{22}-C_{23}-C_{12})]q_2^\mu R+2\sqrt{x_cx_t}C_{24}\gamma^\mu R\}\ ,\end{aligned} \tag{A10}$$

with $C_{ij}(-\hat{p},\hat{q}_2,\hat{M}_W,\hat{M}_W,\sqrt{x_M})$.

The expressions for the form factors for the charged-Higgs-boson contributions to diagrams (b), (d), (f), and (j) in Fig. 1 are given by the following with the same notation conventions as above and the coefficients F_u and F_d are given in Table I;

$$\begin{aligned}B_{H^\pm}^\mu=\frac{g^2}{2\hat{M}_W^2}[&\{2x_M\sqrt{x_c}B_d[F_d^2(C_{11}+C_{21})-F_uF_d(C_0+C_{11})]+2x_t\sqrt{x_c}F_u^2A_d(C_{12}-C_{11}-C_{21}+C_{23})\}p^\mu L\\&+\{2x_M\sqrt{x_c}[F_uF_dB_d(C_{11}+C_0)-F_d^2B_d(C_{12}+C_{23})+F_uF_dA_d(C_{12}-C_{11})]\\&\quad+2x_t\sqrt{x_c}F_u^2A_d(C_{23}-C_{22})\}q_2^\mu L\\&+(x_Mx_cF_uF_d[A_dC_{11}-B_d(C_0+C_{11})]+x_Mx_tF_uF_d[A_d(C_{12}-C_0-C_{11})+B_d(C_{11}-C_{12})]\\&\quad+x_cx_tF_u^2A_dC_{12}+x_MF_d^2\{-x_MA_dC_0+B_d[\tilde{C}_0+(x_c-\hat{p}^2)C_{12}+\hat{p}^2C_{11}-2C_{24}]\})\gamma^\mu L\\&+\{2x_M\sqrt{x_t}[-F_uF_dA_d(C_{11}+C_0)+F_d^2B_d(C_{12}-C_{11}-C_{21}+C_{23})]+2x_c\sqrt{x_t}F_u^2A_d(C_{11}+C_{21})\}p^\mu R\\&+(2x_M\sqrt{x_t}\{F_uF_dA_d(C_{11}+C_0)+B_d[F_d^2(C_{23}-C_{22})+F_uF_d(C_{12}-C_{11})]\}\\&\quad-2x_c\sqrt{x_t}F_u^2A_d(C_{12}+C_{23}))q_2^\mu R\\&+(x_M\sqrt{x_cx_t}\{-F_uF_dA_d(C_0+C_{12})+B_d[F_d^2C_{12}+F_uF_d(C_{12}-C_0)-F_u^2C_0]\}\\&\quad+\sqrt{x_cx_t}F_u^2A_d[\tilde{C}_0+\hat{p}^2C_{11}+(x_c-\hat{p}^2)C_{12}-2C_{24}])\gamma^\mu R]\ ,\end{aligned} \tag{A11}$$

with $C_{ij}(\hat{p},-\hat{q}_2,\sqrt{x_M},\sqrt{x_M},\hat{m}_{H^\pm})$,

$$\begin{aligned}D_{H^\pm}^\mu=\frac{g^2}{2\hat{M}_W^2(x_c-x_t)}\{&[x_c(x_MF_d^2+x_tF_u^2)A_uB_1-x_M(x_c+x_t)F_uF_dA_uB_0]\gamma^\mu L\\&+\sqrt{x_cx_t}[(x_cF_u^2+x_MF_d^2)B_uB_1-2x_MF_uF_dB_uB_0]\gamma^\mu R\}\ ,\end{aligned} \tag{A12}$$

with $B_i(-\hat{q}_1,\sqrt{x_m},\hat{m}_{H^\pm})$,

$$\begin{aligned}F_{H^\pm}^\mu=\frac{g^2}{2\hat{M}_W^2(x_t-x_c)}\{&[x_t(x_MF_d^2+x_cF_u^2)A_uB_1-x_M(x_t+x_c)F_uF_dA_uB_0]\gamma^\mu L\\&+\sqrt{x_cx_t}[(x_tF_u^2+x_MF_d^2)B_uB_1-2x_MF_uF_dB_uB_0]\gamma^\mu R\}\ ,\end{aligned} \tag{A13}$$

with $B_i(-\hat{q}_2\sqrt{x_M},\hat{m}_{H^\pm})$,

$$J_{H^\pm}^{\mu}=\frac{g^2E}{2\hat{M}_W^2}(\{x_M\sqrt{x_c}[-F_d^2(C_0+2C_{21}+3C_{11})-F_uF_d(C_0+2C_{11})]+x_t\sqrt{x_c}F_u^2(C_{11}-C_{12}+2C_{21}-2C_{23})\}p^\mu L$$
$$+\{2x_M\sqrt{x_c}[F_d^2(C_{12}+C_{23})+F_uF_dC_{12}]+2x_t\sqrt{x_c}F_u^2(C_{22}-C_{23})\}q_2^\mu L+2x_MF_d^2C_{24}\gamma^\mu L$$
$$+\{x_M\sqrt{x_t}[F_d^2(C_{11}-C_{12}+2C_{21}-2C_{23})-F_uF_d(C_0+2C_{11})]-x_c\sqrt{x_t}F_u^2(C_0+2C_{21}+3C_{11})\}p^\mu R$$
$$+\{2x_M\sqrt{x_t}[F_d^2(C_{22}-C_{23})+F_uF_dC_{12}]+2x_c\sqrt{x_t}F_u^2(C_{12}+C_{23})\}q_2^\mu R+2\sqrt{x_cx_t}F_u^2C_{24}\gamma^\mu R)\ , \tag{A14}$$

with $C_{ij}(-\hat{p},\hat{q}_2,\hat{m}_{H^\pm},\hat{m}_{H^\pm},\sqrt{x_M})$.

The dot products in Eq. (2.5) are expressed as

$$\hat{q}_1\cdot\hat{q}_2=1/2(x_t+x_c-M_Z^2/M_W^2)\ ,$$
$$\hat{q}_1\cdot\hat{p}=\hat{q}_1\cdot\hat{q}_2-x_c\ , \tag{A15}$$
$$\hat{q}_2\cdot\hat{p}=1/2(M_Z^2/M_W^2+x_t-x_c)\ .$$

We note that these expressions are valid for the flavor-changing transitions of heavy up-type quarks. The expressions for the corresponding decays of heavy down-type quarks are given by the above with the following replacements: $A_u(B_u)\to A_d(B_d)$, $A_d(B_d)\to A_u(B_d)$, the coefficients of the expressions for diagrams (h) and (i) in Fig. 1 change sign to account for the change in sign of the weak isospin of the decaying quark (i.e., $g^2D/2\hat{M}_W\to -g^2D/2\hat{M}_W$), and the coefficients of diagrams (g) and (j) also change sign to account for the change of sign of the electric charge of the internal W boson (i.e., $C\to -C$ and $E\to -E$).

[1] M. K. Gaillard and B. W. Lee, Phys. Rev. D **10**, 897 (1974); E. Ma, *ibid.* **9**, 3103 (1974).

[2] On the subject of B-$\bar{B}$ mixing, see, for example, V. Barger *et al.*, Phys. Lett. B **194**, 312 (1987), and references therein. For rare B decays, see, e.g., W.-S. Hou, A. Soni, and R. S. Willey, Phys. Rev. Lett. **58**, 1608 (1987); **60**, 2337(E) (1988); R. Grigjanis *et al.*, Phys. Lett. B **213**, 355 (1988); **233**, 239 (1989); N. G. Deshpande *et al.*, Phys. Rev. Lett. **57**, 1106 (1986); B. Grinstein, R. Springer, and M. Wise, Phys. Lett. B **202**, 138 (1988); N. G. Deshpande *et al.*, Phys. Rev. Lett. **59**, 183 (1987); S. Bertolini, F. Borzumati, and A. Masiero, *ibid.* **59**, 180 (1987); W. Jaus and D. Wyler, Phys. Rev. D **41**, 3405 (1990); T. Inami and C. S. Lim, Prog. Theor. Phys. **65**, 297 (1981).

[3] See, for example, J. S. Hagelin and L. S. Littenberg, Prog. Nucl. Part. Phys. **23**, 1 (1989); S. Bertolini, F. Borzumati, and A. Masiero, Phys. Lett. **92B**, 437 (1987); G. Eilam *et al.*, Phys. Lett. B **193**, 533 (1987); W.-S. Hou, A. Soni, and H. Steger, *ibid.* **192**, 441 (1987); J. L. Hewett, *ibid.* **193**, 327 (1987); T. G. Rizzo, Phys. Rev. D **38**, 820 (1988); B. Grinstein and M. Wise, Phys. Lett. B **201**, 274 (1988); W.-S. Hou and R. S. Willey, Nucl. Phys. **B326**, 54 (1989).

[4] See, for example, *Proceedings of the Workshop on Science at the KAON Factory,* TRIUMF, Vancouver, Canada, 1990, edited by D. Gill (TRIUMF, Vancouver, 1991); *Workshop Towards Establishing a B Factory,* Proceedings, Syracuse, New York, 1989, edited by M. Goldberg and S. Stone (Syracuse University, Syracuse, 1989).

[5] G. Eilam, B. Haeri, and A. Soni, Phys. Rev. Lett. **62**, 719 (1989); Phys. Rev. D **41**, 875 (1990).

[6] W.-S. Hou and R. G. Stuart, Phys. Rev. Lett. **62**, 617 (1989); Nucl. Phys. **B320**, 277 (1989).

[7] F. Dydak, in *Proceedings of the 25th International Conference on High Energy Physics,* Singapore, 1990, edited by K. K. Phua and Y. Yamaguchi (World Scientific, Singapore, 1991).

[8] N. G. Deshpande and G. Eilam, Phys. Rev. D **26**, 2463 (1982); N. G. Deshpande and M. Nazerimonfared, Nucl. Phys. **B213**, 390 (1983); S.-P. Chia and G. Rajagopal, Phys. Lett. **156B**, 405 (1985); J. M. Soares and A. Barroso, Phys. Rev. D **39**, 1973 (1989); A. Barroso, *ibid.* **42**, 901 (1990).

[9] J. L. Diaz-Cruz *et al.*, Phys. Rev. D **41**, 891 (1990).

[10] B. Dutta Roy *et al.*, Phys. Rev. Lett. **65**, 827 (1990).

[11] H. Fritzsch, Phys. Lett. B **224**, 423 (1989); W. Buchmuller and M. Gronau, *ibid.* **220**, 641 (1989).

[12] CDF Collaboration, L. Pondrom, in *Proceedings of the 25th International Conference on High Energy Physics* [7].

[13] V. Barger, J. L. Hewett, and T. G. Rizzo, Phys. Rev. Lett. **65**, 1313 (1990).

[14] U. Amaldi *et al.*, Phys. Rev. D **36**, 1385 (1987); G. Costa *et al.*, Nucl. Phys. **B297**, 244 (1988); J. Rosner, Phys. Rev. D **42**, 3107 (1990); T. Rizzo, University of Wisconsin Report No. MAD/PH/608, 1990 (unpublished).

[15] W. Hollik, Max-Planck Institute Report No. MPI-PEA/PTh 37/90, 1990 (unpublished); A. Denner, R. J. Guth, and J. H. Kühn, Max-Planck Institute Report No. MPI-PEA/PTh 77/89, 1989 (unpublished); A. Djouadi, J. L. Kneur, and G. Moultaka, Phys. Lett. B **242**, 265 (1990).

[16] M. Strovink, in *Research Directions for the Decade,* Proceedings of the Workshop, Snowmass, Colorado, 1990 (Editions Frontières, Gif-sur-Yvette, in press).

[17] T. L. Barklow, in *Research Directions for the Decade* [16].

[18] M. Kobayashi and T. Maskawa, Prog. Theor. Phys. **49**, 652 (1973).

[19] G. 't Hooft and M. Veltman, Nucl. Phys. **B153**, 365 (1979); G. Passarino and M. Veltman, *ibid.* **B160**, 151 (1979); A. Axelrod, *ibid.* **B209**, 349 (1982).

[20] S. L. Glashow, J. Iliopoulos, and L. Maiani, Phys. Rev. D **2**, 1285 (1970).

[21] See, for example, V. Barger and R. J. N. Phillips, *Collider Physics* (Addison-Wesley, New York, 1987).

[22] Particle Data Group, J. J. Hernández *et al.*, Phys. Lett. B **239**, 1 (1990).
[23] For a recent review, see S. Dawson *et al.*, *The Higgs Hunter's Guide* (Addison-Wesley, Reading, MA, 1989).
[24] V. Barger, J. L. Hewett, and R. J. N. Phillips, Phys. Rev. D **41**, 3421 (1990); see also A. J. Buras *et al.*, Nucl. Phys. **B337**, 284 (1990); J. F. Gunion and B. Grzadkowski, Phys. Lett. B **243**, 301 (1990).
[25] J. Lopez and D. V. Nanopoulos, Nucl. Phys. **B338**, 73 (1990); S. Kelley, J. Lopez, and D. V. Nanopoulos, Texas A&M University Report No. CTP-TAMU-90-90, 1990 (unpublished).
[26] G. Eilam, J. L. Hewett, and A. Soni (unpublished).
[27] R. S. Willey and H. L. Yu, Phys. Rev. D **26**, 3086 (1982).
[28] T. G. Rizzo, Phys. Rev. D **35**, 1067 (1987); V. Barger and W.-Y. Keung, Phys. Lett. B **202**, 393 (1988).
[29] V. Barger (private communication).